Conference paper

Petr Janicek*, Stanislav Slang, Karel Palka and Miroslav Vlcek

Spectroscopic ellipsometry characterization of spin-coated $Ge_{25}S_{75}$ chalcogenide thin films

DOI 10.1515/pac-2016-1019

Abstract: Spectroscopic ellipsometry study on spin-coated non-toxic $Ge_{25}S_{75}$ thin films annealed at different temperatures were conducted. Multi sample analysis with two sets of samples spin-coated onto soda-lime glass and onto silicon wafers was utilized. Optical constants (refractive index n and extinction coefficient k) of these films were determined from ellipsometric data recorded over a wide spectral range (0.05–6 eV). Different parametrization of $Ge_{25}S_{75}$ complex dielectric permittivity which consists of a Tauc-Lorentz or Cody-Lorentz oscillator describing the short wavelength absorption edge, a Lorentz or Gauss oscillators describing phonon absorption or optically active absorption of alkyl ammonium germanium salts in the middle infrared part of spectra is discussed. Using a Mott-Davis model, the decrease in local disorder with increasing annealing temperature is quantified from the short wavelength absorption edge onset. Using the Wemple-DiDomenico single oscillator model for the transparent part of the optical constants spectra, a decrease in the centroid distance of the valence and conduction bands with increasing annealing temperature is shown and increase in intensity of the inter-band optical transition due to annealing temperature occurs. Intensity of absorption near 3000 cm^{-1} could be used as alternative method to evaluation of quality of prepared films.

Keywords: amorphous chalcogenides; optical properties; spectroscopic ellipsometry; spin-coating; SSC-2016.

Highlights

- Influence of annealing temperature on properties of $Ge_{25}S_{75}$ thin films is studied.
- Discussion of different models for evaluation of ellipsometric data.
- Application of Wemple-DiDomenico and Mott-Davis model.

Introduction

Chalcogenide glasses are semiconductor optical materials with promising potential especially in infrared optics [1–4]. Great effort has been invested into research of non-toxic chalcogenide glasses which could be

Article note: A collection of invited papers based on presentations at the 12th Conference on Solid State Chemistry (SSC-2016), Prague, Czech Republic, 18–23 September 2016.

***Corresponding author: Petr Janicek,** Institute of Applied Physics and Mathematics, Faculty of Chemical Technology, University of Pardubice, Studentska 95, Pardubice 53210, Czech Republic; and Center of Materials and Nanotechnologies, Faculty of Chemical Technology, University of Pardubice, Studentska 95, Pardubice 53210, Czech Republic, e-mail: petr.janicek@upce.cz
Stanislav Slang and Miroslav Vlcek: Center of Materials and Nanotechnologies, Faculty of Chemical Technology, University of Pardubice, Studentska 95, Pardubice 53210, Czech Republic
Karel Palka: Department of General and Inorganic Chemistry, Faculty of Chemical Technology, University of Pardubice, Studentska 95, Pardubice 53210, Czech Republic; and Center of Materials and Nanotechnologies, Faculty of Chemical Technology, University of Pardubice, Studentska 95, Pardubice 53210, Czech Republic

mass produced by coating or printing techniques [5, 6]. Major disadvantage of these solution based deposition methods is the content of residual solvent molecules remaining in the thin film's structure, which can be significantly decreased by proper post-deposition annealing [7]. In our previous study successful preparation of spin-coated non-toxic $Ge_{25}S_{75}$ chalcogenide thin films were demonstrated [8].

Properties of Ge-S systems prepared by thermal evaporation were studied in the past [9, 10] and the blue shift of the optical bandgap energy induced by annealing accompanied by an increase in both short- and medium range order is reported. Photo induced phenomena in these films were further studied e.g. by Munzar et al. [11] and Knotek et al. [12]. Structure and optical properties of amorphous GeS_x films prepared by pulsed laser deposition were studied by Pan et al. [13].

Amorphous chalcogenides possess high refractive index (~2.5; 2.8; 3.0 for sulfides, selenides and tellurides, respectively) [4] and are transparent in wide spectral range (from wavelength around 400–600 nm to about up to 10, 15, 20 μm for majority of sulfides, selenides and tellurides, respectively) [4]. The range of transparency of these materials is limited by short wavelength absorption edge (SWAE) on the one side and by long wavelength absorption edge on the other side. In the literature e.g. [14], different models are used for description of SWAE. Commonly, Tauc-Lorentz oscillator (TL) [15, 16]

$$\begin{aligned}
\varepsilon_2 &= \frac{A\cdot E_0\cdot C\cdot (E-E_g^{opt}(\mathrm{TL}))^2}{(E^2-E_0^2)^2+C^2\cdot E^2}\cdot\frac{1}{E}\,\text{for}\,E>E_g^{opt}(\mathrm{TL})\\
\varepsilon_2 &= 0\,\text{for}\,E\le E_g^{opt}(\mathrm{TL})\\
\varepsilon_1 &= \frac{2}{\pi}P\int_{E_g}^{\infty}\frac{\xi\cdot\varepsilon_2(\xi)}{\xi^2-E^2}d\xi
\end{aligned} \tag{1}$$

is used for parametrization of SWAE of amorphous materials. In this model, film is transparent below E_g^{opt} (TL) (called optical bandgap). This value is usually estimated from so called Tauc plot from transmission measurement. Other used parameters A, E_0, C stand for amplitude, peak position and broadening of the oscillator, respectively.

Instead of Tauc-Lorentz, Cody-Lorentz oscillator (CL) [17] can be used.

$$\begin{aligned}
\varepsilon_2 &= \frac{E_1}{E}\exp\left(\frac{E-E_g^{opt}(\mathrm{CL})-E_t}{E_u}\right)\text{for}\,0<E<(E_g^{opt}(\mathrm{CL})+E_t)\\
\varepsilon_2 &= G(E)L(E)=\frac{(E-E_g^{opt}(\mathrm{CL}))^2}{(E-E_g^{opt}(\mathrm{CL}))^2+E_p^2}\cdot\frac{AE_0\Gamma E}{\left[(E^2-E_0^2)^2+\Gamma^2E^2\right]}\,\text{for}\,E>(E_g^{opt}(\mathrm{CL})+E_t)\\
\varepsilon_1 &= E_tG(E)L(E)
\end{aligned} \tag{2}$$

CL parametrization is similar to the TL in that it defines the optical bandgap energy E_g^{opt} (CL). The Cody-Lorentz model also includes an Urbach absorption term. Disadvantage of this model is higher number of free parameters in comparison with TL model.

As was mentioned earlier, major disadvantage of solution based deposition techniques is the residual amount of solvent remaining in the thin film's structure. But its content can be significantly lowered by proper annealing [7, 18, 19]. Residual amount of solvent could be optically active (absorbs light) and can be modeled by Lorentz oscillator [20]. For the modeling purpose of these absorptions in amorphous materials, the Gauss oscillator [21, 22] is commonly used as well. This paper deepens the results published in our previous paper where spin-coated non-toxic thin films of $Ge_{25}S_{75}$ were prepared and studied for the first time [8].

In our work, results obtained by spectroscopic ellipsometry are in detail discussed to study the optical properties of spin-coated $Ge_{25}S_{75}$ annealed at various temperatures. Different models of amorphous $Ge_{25}S_{75}$ films are used and discussed with the utilization of multi sample analysis. The effects of annealing temperature on the complex dielectric functions are investigated over a broad spectral range from 0.05 to 6 eV. In the vicinity of the absorption edge ($3.0<E<4.0$ eV) a Mott-Davis model, in the semi-transparent

spectrum ($0.5 < E < 2.5$ eV) a Wemple-DiDomenico single oscillator dispersion, and in the mid-infra-red (MIR) ($0.05 < E < 0.5$ eV) a Gauss or Lorentz oscillator model were employed as this analysis provide physical meaning of the extracted parameters.

Experimental details

The source bulk $Ge_{25}S_{75}$ chalcogenide glass was prepared by standard melt-quenching method. High purity (5N) elements were loaded into the quartz ampule in appropriate amounts and sealed under vacuum ($\sim 10^{-3}$ Pa). The glass synthesis was performed in rocking tube furnace at 950 °C for 72 h. The ampule with melted glass was quenched in cold water.

Prepared bulk glass was grinded in agate bowel and dissolved in n-butylamine (BA) with concentration 0.075 g of glass powder per 1 mL of BA solvent. The thin films were deposited using spin-coating method (spin-coater Best Tools SC110) onto soda-lime glass substrates and onto silicon substrates with native SiO_2 layer (with 2000 rpm for 120 s under argon atmosphere where substrate have temperature 21 °C the same as ambient temperature) yielding thin films of good optical quality. Immediately after deposition the thin films were stabilized by annealing at 60 °C for 20 min on a hot plate in ambient atmosphere (hereinafter referred as as-prepared thin film). Deposited samples were stored in dry and dark environment.

Samples of as-prepared thin films were annealed at temperatures 90 °C (t90), 120 °C (t120), 150 °C (t150), 180 °C (t180), 210 °C (t210) and 240 °C (t240) °C for 60 min on annealing table (Conbrio, Czech Republic) inside argon filled annealing chamber. The highest annealing temperature used in our study 240 °C is sufficiently bellow glass-transition temperature reported to be 360 °C [23] to rule out possible seeding of crystallites.

Two variable angle spectroscopic ellipsometers (VASE and IR-VASE J. A. Woollam Co.) were used for the optical characterization of the prepared samples. The first ellipsometer was equipped with an automatic rotating analyzer over the spectral range 210 nm–1700 nm (UV-VIS-NIR), measuring 30 revolutions with photon energy steps of 0.05 eV at three selected angles of incidence (AOI) (50°, 60° and 70°). The second ellipsometer was equipped with a rotating compensator for 1.7–22 μm (NIR-MIR), using same AOI, measuring 25 scans, 15 spectra per revolution with wavenumber steps 8 cm^{-1}. Near normal incidence optical reflectance was measured by the same instruments. Optical spectrometer (Shimadzu UV3600) was used for transmission spectra measurements in the spectral region 190–2000 nm. WVASE32 software was used for evaluation the measured data.

Results and discussion

Structure model and material optical constants

Two sets of samples were prepared by the same spin-coating procedure on different substrates. As shown in Fig. 1 (left column), a sample model used to analyze the raw ellipsometry data consists of i) a semi-infinite

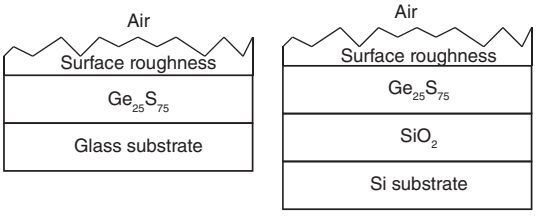

Fig. 1: Sketch of the optical models used to fit the ellipsometry data.

glass substrate, ii) a homogenous, isotropic layer representing the $Ge_{25}S_{75}$ film, iii) surface roughness and iv) air as the ambient medium. Analogously in Fig. 1 (right column), a sample model consists of i) a crystalline silicon substrate, ii) a SiO_2 layer, iii) a homogenous, isotropic layer representing the $Ge_{25}S_{75}$ film, iv) surface roughness and v) air as the ambient medium.

For ellipsometry and reflectivity measurements of samples on glass substrates, their backside was roughened to avoid unwanted backside reflection. Optical constants of the glass substrate were obtained by measurement of an uncoated glass substrate. In case of Si substrate backside reflection was treated in the WVASE32 software numerically. Possible thickness nonuniformity was modeled in the WVASE32 software as well.

Optical constants of Si and SiO_2 in the NIR – VIS – UV range were taken from the literature [24]. Optical constants of Si and SiO_2 layer in the MIR part of spectra was obtained by measurement of an uncoated SiO_2/Si substrate.

In this work, different model dielectric function, TL or CL model describing SWAE and sum of Lorentz or Gauss oscillators representing absorption in middle infrared part of spectra will be used and compared. Therefore model dielectric function used for the $Ge_{25}S_{75}$ films consists of several contributions:

$$\tilde{\varepsilon} = \tilde{\varepsilon}_{\mathrm{TL}} / \tilde{\varepsilon}_{\mathrm{CL}} + \sum \tilde{\varepsilon}_{\mathrm{Lorentz}} / \tilde{\varepsilon}_{\mathrm{Gauss}} \tag{3}$$

Surface roughness is modeled by a Bruggeman type effective medium approximation [25] with 50 % of voids and 50 % of $Ge_{25}S_{75}$. With the aim to improve reliability of obtained results, multi sample analysis has been employed with simultaneous use of samples spin-coated onto glass substrate and onto silicon substrate in the fitting procedure.

Figure of merit and quality of the fit

The change of the polarization state is usually expressed by two parameters, amplitude ratio ψ and phase shift Δ, that are defined using the Fresnel reflection coefficients for *p*- and *s*- polarized light:

$$\frac{r_p}{r_s} = \tan(\psi) \cdot \exp(\mathrm{i}\Delta) \tag{4}$$

Spectroscopic ellipsometry is an indirect optical characterization method, where the measured values ψ_{exp} and Δ_{exp} are compared to the values calculated from the model. In the model structure, the model dielectric function which define optical constants of the layers and their thicknesses are assumed, and corresponding values of ψ_{mod} and Δ_{mod} belonging to the proposed model structure are calculated. In this way, the optical parameters of studied layers, such as complex refractive index (which includes refractive index as the real part and extinction coefficient as the imaginary part) together with geometrical properties (such as thickness of the layer and surface roughness) can be calculated.

In our case, the measured spectroscopic ellipsometry parameters, ψ^{exp} and Δ^{exp} fitted against the designed model in the spectral range from 0.05 eV to 6 eV using the mean square error (MSE) given in the following expression:

$$MSE = \sqrt{\frac{1}{2N-M} \sum_{i=1}^{N} \left[\left(\frac{\psi_i^{\mathrm{mod}} - \psi_i^{\mathrm{exp}}}{\sigma_{\psi,i}^{\mathrm{exp}}} \right)^2 + \left(\frac{\Delta_i^{\mathrm{mod}} - \Delta_i^{\mathrm{exp}}}{\sigma_{\Delta,i}^{\mathrm{exp}}} \right)^2 \right]} \tag{5}$$

where N is the number of measured pairs of ellipsometric parameters ψ^{exp} and Δ^{exp} and M represents the total number of fitted parameters. $\sigma_{\psi,i}^{\mathrm{exp}}$ and $\sigma_{\Delta,i}^{\mathrm{exp}}$ are then the estimated experimental error of ψ^{exp} and Δ^{exp}, respectively. Ellipsometric data measured for all three angles of incidence 50°, 60° and 70° were used in the fit simultaneously. Moreover, multi sample analysis consisting the $Ge_{25}S_{75}$ films with the same optical constants

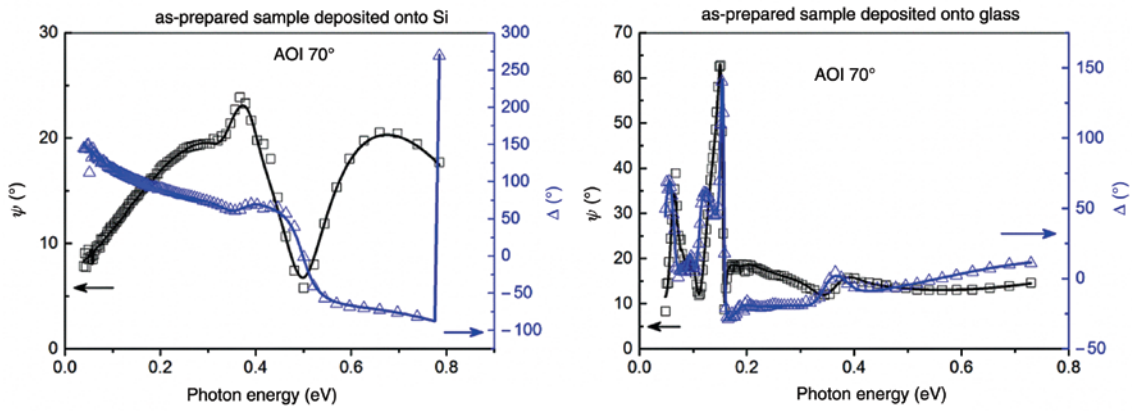

Fig. 2: Measured values of ψ (circles) and Δ (triangles) for as-prepared $Ge_{25}S_{75}$ sample in the MIR part of the spectrum for sample deposited onto Si substrate (left column) and for sample deposited onto glass substrate (right column). The best fit for the angle of incidence 70° is shown by solid lines.

parametrization on two different substrates were used in the fit. Data from optical reflectivity and optical transmission were used in the fit as well with the use of MSE in the similar manner as described in eq. 5.

Figure 2 shows the comparison of ellipsometry parameters, ψ (circles) and Δ (triangles) for an AOI of 70° in the spectral range from 0.05 to 0.8 eV (MIR part of spectrum) for $Ge_{25}S_{75}$ as-prepared onto Si substrate (left column) and for $Ge_{25}S_{75}$ as-prepared onto glass substrate (right column).

Based on proposed model described in details later, transmission and reflectivity could be calculated and used in the fit as well. Sufficient fit quality of the transmission and reflectivity data can be seen at Fig. 3. Incorporation of the transmission data into the fit improve reliability of calculated optical constants especially in the region close to the bandgap.

Film thickness and surface roughness

Measurement of the uncoated SiO_2/Si substrate revealed a native SiO_2 layer thickness of 2 nm. Measured thicknesses of $Ge_{25}S_{75}$ films are summarized in Table 1.

Although thickness of the films deposited onto glass substrate and onto Si substrate slightly differs, its dependence on annealing temperature is similar. The similar huge thickness decrease (approximately to the

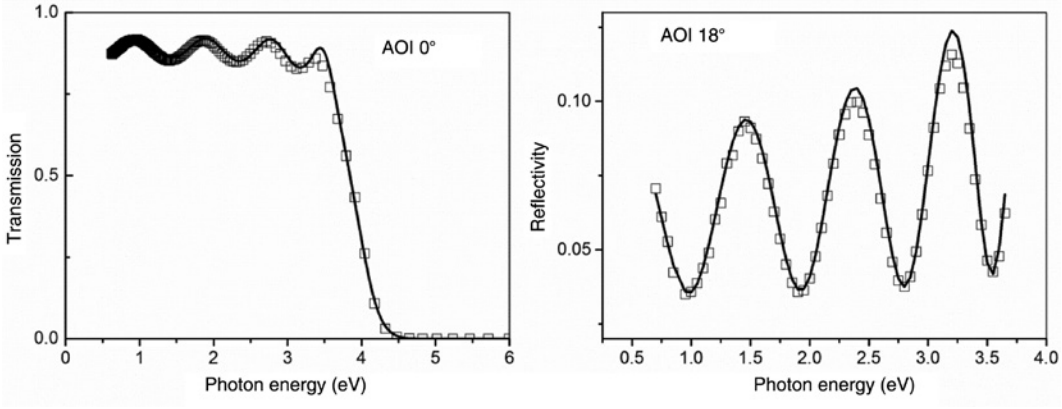

Fig. 3: Measured values of transmission (symbols, left column) and reflectivity (symbols, right column) for t90 sample in the NIR-VIS-UV part of the spectra for sample deposited onto glass substrate. The best fit is shown by solid lines.

Table 1: Thickness, surface roughness and thickness nonuniformity of $Ge_{25}S_{75}$ films spin-coated onto soda-lime glass and Si substrates obtained by the best fit of ellipsometry data using Tauc-Lorentz parametrization.

Sample	Thickness of samples (on glass substrate) (nm)	Thickness of samples (on Si substrate) (nm)	Surface roughness (on glass substrate) (nm)	Surface roughness (on Si substrate) (nm)	Thickness nonuniformity (%)
as-prepared	396.0±0.2	444.0±0.2	0.3±0.1	2±2	5.0±0.5
t-90 °C	378.9±0.2	436.2±0.2	0.9±0.1	0±2	9.1±0.5
t-120 °C	345.2±0.2	367.8±0.2	2.3±0.1	1.2±0.7	8.3±0.3
t-150 °C	260.1±0.2	306.0±0.2	5.5±0.1	6±1	6.4±0.4
t-180 °C	220.0±0.2	223.9±0.2	5.1±0.1	7±2	3.8±0.4
t-210 °C	197.5±0.2	197.5±0.2	11.2±0.1	12.5±0.3	3.2±0.4
t-240 °C	189.3±0.2	183.1±0.2	12.8±0.1	13±1	4.0±0.5

half) caused by annealing temperature as in the studied case has been reported previously for As_2S_3 spin-coated layers [26] and was explained by releasing of organic residues and by the glass densification.

In our previous paper [8] good agreement between surface roughnesses determined by spectroscopic ellipsometry on the samples prepared on soda-lime glass substrate and surface roughnesses determined by AFM was shown. Moreover AFM scans do not reveal any signs of seeding of crystallites. As can be seen from Table 1 surface roughness is only slightly dependent on the used substrate. Increase of surface roughness with the annealing temperature observed on both used substrates is connected with releasing of alkyl ammonium germanium salts residue from the films together with decreasing of film thickness.

Thicknesses of the films obtained by CL model are nearly the same within experimental error less than 1%. The values of thickness nonuniformity obtained by the fit of measured depolarization parameter are presented in the Table 1 and reflect possible wedging of the film.

It is worth to mention that stoichiometry of the samples is slightly changing. The gradual decrease of the sulfur content with increasing annealing temperature has been observed (see Fig. 7 at Ref. [8]). The composition after annealing at 240 °C obtained by EDS measurement is $Ge_{29,1}S_{70,9}$.

Refractive index and extinction coefficients of $Ge_{25}S_{75}$ in wide spectral range

Figure 4 shows determined wide spectral range dispersion of the refractive index, n, and extinction coefficient, k, of $Ge_{25}S_{75}$ films annealed on different temperature. In the NIR-VIS-UV region ($0.5 < E < 6.0$ eV) all

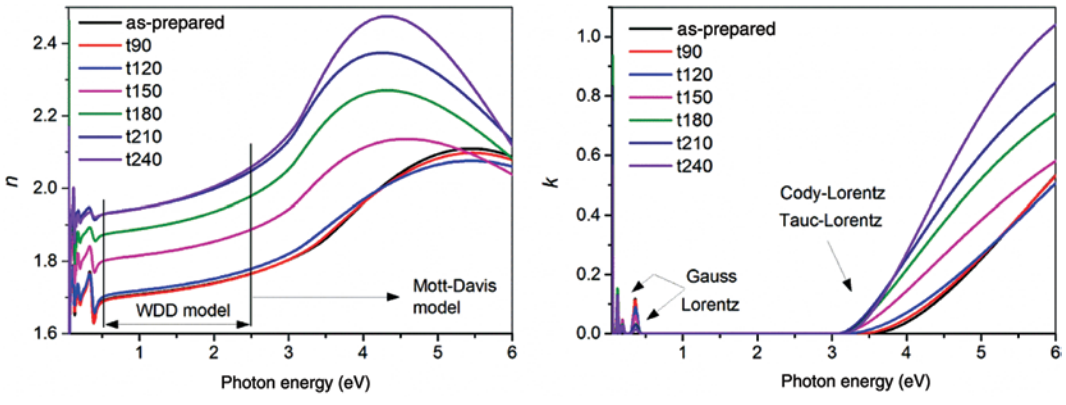

Fig. 4: Determined $Ge_{25}S_{75}$ refractive index n (left column), and extinction coefficient k (right column), as a function of photon energy in the wide spectral range. Indication of spectral ranges where different models [Mott-Davis, Wemple-DiDomenico (WDD)] are used (left), indicate the different oscillators used (right).

samples show a broad profile of refractive index with a peak moving towards lower photon energies (red shift) with the increasing annealing temperature. The refractive index is increasing with the annealing temperature suggesting densification of glass structure at elevated annealing temperatures. It is probable that as-prepared samples exhibits residual tensile stress and with the increasing annealing temperature stress relaxation takes place influencing refractive index as well. Although existence of the nano pores in the spin-coated $Ge_{23}Sb_7S_{70}$ thin films [27] and in ion sputtered TaO_5 coatings [28] were reported in the literature there is no direct evidence of nano pores in studied films.

In the NIR-VIS-UV region, SWAE is present. The onset of SWAE is moving toward lower photon energies consistently with described shift of refractive index peak with the exception of t240 sample. Relationship between real (refractive index n) and imaginary (extinction coefficient k) part of complex refractive index is described by Kramers–Kronig relations [29, 30]. The extinction coefficient of all samples is ~ 0 in the visible spectrum.

In the MIR region ($0.05 < E < 0.5$ eV), optical active absorptions either from alkyl ammonium germanium salts residues or from absorption of photons by phonons are present.

In the following sections the wide spectral range of $Ge_{25}S_{75}$ refractive index and extinction coefficient will be divided into three parts (as shown in Fig. 4) where different models (Mott-Davis, Wemple-DiDomenico) will be applied to get more physical insight.

Effect of annealing temperature on the refractive index dispersion data

The effect of annealing temperature on the refractive index dispersion data in the semi-transparent part of spectra below the bandgap ($0.5 < E < 2.5$ eV) is further investigated using a Wemple-DiDomenico model [31, 32]. The refractive index data can be fitted in this spectral range to the single oscillator expression

$$n^2(E) = 1 + \frac{E_0 \cdot E_d}{E_0^2 - E^2} \tag{6}$$

where E is the photon energy, E_0 is the energy of the effective dispersion oscillator and E_d is the dispersion energy. From linear regression of dependence $(n^2 - 1)^{-1}$ against E^2 (as shown in Fig. 5), the parameters E_d and E_0 could be calculated.

The parameter E_d, which is a measure of the intensity of the inter-band optical transition, is related to other physical parameters of the material through the following empirical relationship [31, 32],

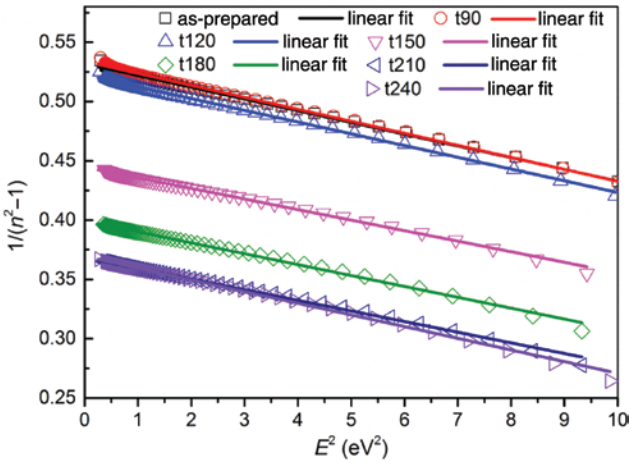

Fig. 5: Dependence of $1/(n^2 - 1)$ as a function of square photon energy obtained from ellipsometry (symbols) and linear fit of this data (solid lines) according to Wemple-DiDomenico model.

$$E_d(\text{eV}) = \beta \cdot N_c \cdot N_e \cdot Z_a \tag{7}$$

where N_c is the effective coordination number of the cation nearest-neighbor to the anion, Z_a is the formal chemical valence of the anion, N_e is the effective number of valence electrons per anion and β is a two valued constant with either an ionic or covalent value ($\beta_{ionic} = 0.26 \pm 0.03$ eV and $\beta_{covalent} = 0.37 \pm 0.04$ eV).

Figure 6 shows the variation of E_d and E_0 as a function of annealing temperature of the $Ge_{25}S_{75}$ films. E_d is ~14 eV for annealing temperatures below 120 °C and ~17 eV for higher annealing temperatures. In spite of eq. 7, increase of E_d could be explained both by increase of β and by increase of N_e. These findings supports results obtained from Raman measurements [8] and could be explained by alkyl ammonium germanium salt releasing from the structure and thermo-induced polymerization connected with changes of local arrangement. Annealing temperature about 150 °C is sufficient for the majority of these changes.

E_0 is ~7.3 eV for as-prepared film and is decreasing with annealing temperature. Parameter E_0 is associated with distance of centroids of valence and conduction band and therefore with optical bandgap ($E_0 \approx 1.5 + 1.25 E_g^{opt}$) [33, 34]. From the decrease of the parameter E_0 with increasing annealing temperature, the decrease in the optical bandgap (red shift) could be deduced. Red shift of optical bandgap with increasing annealing temperature is described for other spin-coated systems e.g. [35] and was explained by increasing density of the spin-coated film reflecting increasing of film refractive index.

Effect of annealing temperature on the optical bandgap

According to the Mott and Davis [36, 37] and Tauc [38] models, the width of the localized states near the mobility edges depends on the degrees of disorder and defects present in the amorphous structure, in particular, differences in coordination number in amorphous state with respect to crystalline state [39, 40].

For photon energies (2.0 eV < E < 6.0 eV) SWAE is observed. As mentioned previously, Tauc-Lorentz oscillator or Cody-Lorentz oscillators are used to model the band edge region.

For majority of amorphous semiconductors, the optical absorption in the vicinity of the SWAE obeys the Tauc relationship [38]:

$$\alpha E = B \cdot (E - E_g^{opt})^2 \tag{8}$$

where $\alpha = \frac{4\pi k}{\lambda}$ is absorption coefficient, E is the energy of the incident photon, B is a constant and E_g^{opt} is the optical energy gap.

In order to obtain parameters from previous equation, dependence in the form of $(\alpha E)^{1/2}$ as a function of photon energy E is depicted at Fig. 7 (left) for Tauc-Lorentz oscillator and at Fig. 7 (right) for Cody-Lorentz

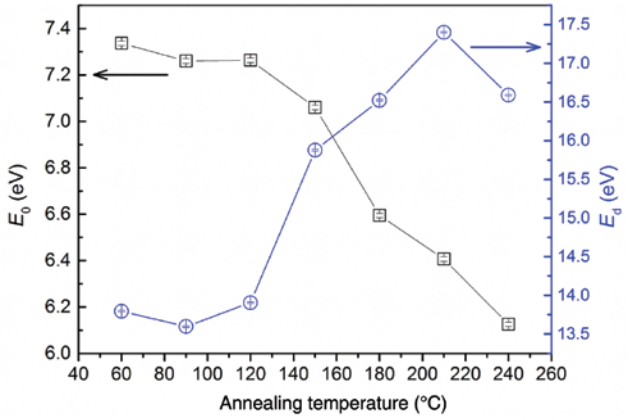

Fig. 6: Wemple-DiDomenico parameters E_d and E_0 as a function of annealing temperature.

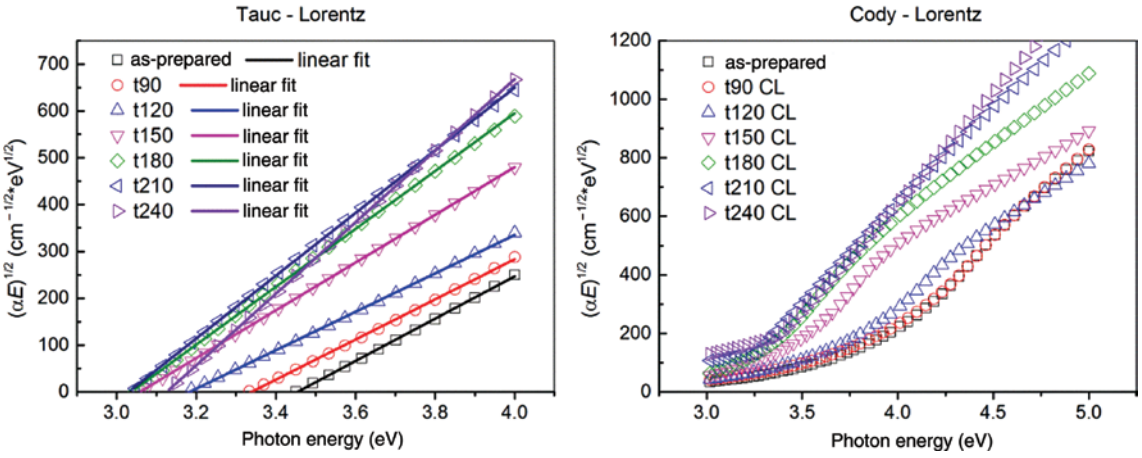

Fig. 7: $(\alpha E)^{1/2}$ as a function of photon energy (symbols, left column) obtained using Tauc-Lorentz oscillator and its linear part described by Tauc model (solid lines, left column). $(\alpha E)^{1/2}$ as a function of photon energy obtained using Cody-Lorentz oscillator (symbols, right column).

oscillator. The Tauc model (eq. 8) is used to describe its linear part (left, lines). Parameter B can be calculated as $B = \frac{4\pi\sigma_{\min}}{nc\Delta E}$ [37], where $\sigma_{\min}$ is the minimum metallic conductivity usually assumed as constant $\approx 350\ \Omega^{-1}\text{cm}^{-1}$, n is the refractive index, c is the free space velocity of light and $\Delta E_c = \Delta E_v = \Delta E$ is the width of localized states near valence band mobility edge can be taken as a measure of a disorder.

Influence of the annealing temperature leads to the considerable changes in the sample disorder (the change of parameter $B^{1/2}$). The width of localized states can be compared with as-prepared sample for all measured samples as $(\Delta E_{tx}/\Delta E_{\text{as-prepared}}) = (B_{\text{as-prepared}}/B_{tx})/(n_{tx}/n_{\text{as-prepared}})$. Table 2 summarizes the change of the slope of SWAE, values of the refractive index for 3.0 eV used for calculation of ΔE ratio together with the results of this calculation.

From these results (Table 2), shrinking of the width of localized states due to annealing temperature can be observed. Annealing temperature 240 °C decrease disorder in the material approximately to 1/3 in comparison with as-prepared sample.

The comparison of TL and CL oscillator is depicted at Fig. 7 (left column Tauc-Lorentz, right column Cody-Lorentz oscillator). The main difference is that CL parametrization allows optical transitions in the bandgap (tail states) and dependence of $(\alpha E)^{1/2}$ as a function of photon energy is not linear above the bandgap. Generally the results obtained by CL model are very close to that obtained by TL model. For comprehensive discussion of these two oscillators parameters of TL model together with MSE are summarized in the Table 3, parameters of CL model together with MSE in the Table 4.

As can be seen from Table 4, CL model exhibits serious difficulties when use for the fitting of SWAE of studied samples. For example parameter E_t describing optical transitions in the bandgap has to be fixed or

Table 2: $B^{1/2}$ = Slope of linear part of the $(\alpha E)^{1/2}$ dependence as a function of photon energy E obtained using Tauc-Lorentz oscillator, n (3.0 eV) = refractive index for 3.0 eV, and comparison of the width of localized states to as-prepared sample.

Sample	$B^{1/2}$ (TL) (cm$^{-1/2}$·eV$^{-1/2}$)	n (3.0 eV)	$\Delta E_{tx}/\Delta E_{\text{as-prepared}}$
as-prepared	452 ± 2	1.85 ± 0.01	–
t-90 °C	480 ± 2	1.84 ± 0.01	0.89 ± 0.01
t-120 °C	446 ± 2	1.84 ± 0.01	1.03 ± 0.01
t-150 °C	502 ± 1	1.95 ± 0.01	0.77 ± 0.01
t-180 °C	586 ± 1	2.06 ± 0.01	0.53 ± 0.01
t-210 °C	640 ± 1	2.14 ± 0.01	0.43 ± 0.01
t-240 °C	745 ± 1	2.18 ± 0.01	0.31 ± 0.01

Table 3: Parameters of TL model together with obtained MSE for all studied samples.

Sample	A^{TL} (eV)	C^{TL} (eV)	E_n^{TL} (eV)	E_g^{opt} (TL) (eV)	MSE^{TL}
as-prepared	83 ± 1	6.8 ± 0.1	7.24 ± 0.03	3.45 ± 0.01	1.6
t-90 °C	77 ± 1	6.9 ± 0.1	7.33 ± 0.03	3.34 ± 0.01	1.6
t-120 °C	78 ± 2	9.2 ± 0.3	7.86 ± 0.05	3.18 ± 0.01	1.5
t-150 °C	98 ± 13	11 ± 2	6.4 ± 0.4	3.06 ± 0.02	1.5
t-180 °C	152 ± 2	11.3 ± 2	5.63 ± 0.05	3.04 ± 0.01	1.4
t-210 °C	156 ± 7	8.9 ± 0.2	5.3 ± 0.2	3.03 ± 0.01	1.8
t-240 °C	152 ± 7	5.9 ± 0.2	5.0 ± 0.1	3.13 ± 0.01	2.2

Table 4: Parameters of CL model together with obtained MSE for all studied samples (superscript fixed means fixed parameter).

Sample	A^{CL} (eV)	E_n^{CL} (eV)	Γ^{CL} (eV)	E_g^{opt} (CL) (eV)	E_p^{CL} (eV)	E_t^{CL} (eV)	E_u^{CL} (eV)	MSE^{CL}
as-prepared	10 ± 2	7.1 ± 0.3	3.3 ± 0.6	4.0 ± 0.2	0.4 ± 0.2	0.4^{fixed}	0.28 ± 0.01	2.6
t-90 °C	10 ± 3	7.0 ± 0.4	3 ± 1	4.0 ± 0.3	0.4 ± 0.4	0.4^{fixed}	0.30 ± 0.01	3.9
t-120 °C	10 ± 3	7.4 ± 0.5	3.3 ± 0.7	3.8 ± 0.2	0.3 ± 0.2	0.4^{fixed}	0.28 ± 0.01	4.3
t-150 °C	24.4 ± 0.4	9.0 ± 0.1	4.7 ± 0.3	3.50 ± 0.03	0.29 ± 0.03	0.3 ± 0.5	0.21 ± 0.01	2.2
t-180 °C	31 ± 1	8.8 ± 0.2	7.1 ± 0.5	3.20 ± 0.02	0.66 ± 0.05	0.3 ± 0.7	0.18 ± 0.01	2.8
t-210 °C	46 ± 3	7.8 ± 0.1	11 ± 2	3.04 ± 0.01	1.43 ± 0.07	0.21 ± 0.01	0.62 ± 0.02	2.0
t-240 °C	75 ± 10	5.2 ± 0.3	11^{fixed}	3.08 ± 0.01	2.6 ± 0.3	0.29 ± 0.01	0.52 ± 0.02	2.6

has significant error in the case of nearly all studied samples. Taking into account that CL parametrization have seven free parameters and TL only four free parameters and that the MSE for CL model is generally higher than for TL model it is more accurate to use Tauc-Lorentz oscillator for the studied samples.

Among all presented parameters usually value of parameter E_g^{opt} is of special importance because it determines range of the transparency. From the transmission measurements E_g^{opt} is usually obtained as interception of linear part of dependence of $(\alpha E)^{1/2}$ as a function of photon energy E with the energy axis. In the TL parametrization this parameter is included (see eq. 1). Parameter E_g^{opt} (TL) obtained from TL model [15, 16] is presented in the Table 3 and can compared with parameter E_g^{opt} (CL) obtained from CL model (see eq. 2) [17].

Consistently both parameters E_g^{opt} (TL) and E_g^{opt} (CL) are generally decreasing with annealing temperature as expected from parameter E_0 (see Fig. 6) with exception of the last sample t240. On vacuum deposited samples, blue shift of optical bandgap was reported [9, 10] leading us to the idea that in our case two mechanism can be proposed for studied spin-coated samples a) decomposition of alkyl ammonium germanium salt molecules connected with decreasing of film thickness and increase of film density and b) thermo-induced structural polymerization. The former influence red shift of E_g, the later blue shift [9, 10, 35]. Very likely both of these mechanisms take part, decomposition of alkyl ammonium germanium salt molecules prevails for lower annealing temperatures, thermo-induced polymerization takes pronounced place for higher annealing temperatures. Moreover stress relaxation induced by annealing temperature could be presented as well.

Effect of annealing temperature in the MIR part of spectra

As was mentioned earlier, in the MIR part of spectra, optically active absorptions of alkyl ammonium germanium salts and absorptions of photons by phonons are present. Usually Lorentz oscillators are used for this type absorption. In case of amorphous materials, gauss oscillator can be used instead. The refractive index comparison of both oscillators used for the sample annealed at the lowest (as-prepared) and the highest (t240) temperature is depicted at Fig. 8. Usage of both oscillators leads to very similar results. For amorphous samples, use of gauss oscillator is usually preferred allowing to model broader absorption peak (Gaussian widening of the Lorentz oscillators).

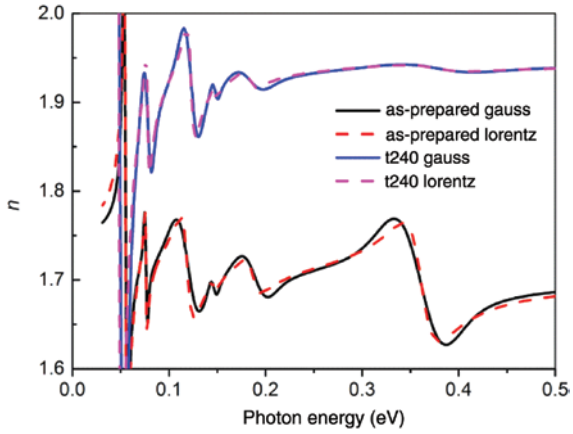

Fig. 8: Comparison of refractive index in MIR part of spectra calculated by Gauss and Lorentz oscillators.

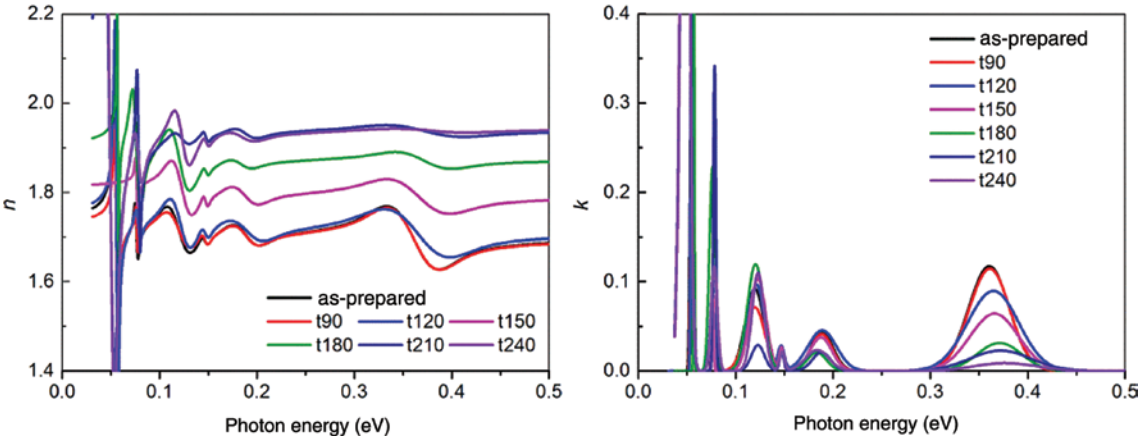

Fig. 9: Determined $Ge_{25}S_{75}$ refractive index n (left column), and extinction coefficient k (right column), as a function of photon energy in MIR part of spectra.

Refractive index, respectively extinction coefficient of all studied films obtained using Gauss oscillators are depicted in the Fig. 9.

From the results of Raman measurement described in our previous paper [8] some of these absorptions (especially that close to 3000 cm^{-1}) can be associated with alkyl ammonium germanium sulfide salts molecules. As we shown [8] intensity of this particular absorption matches well with results of EDS analysis and therefore infrared ellipsometry could be used as alternative method for determine of quality of annealed spin-coated films. Described intensity of absorption peak close to 3000 cm^{-1} is still not negligible even for the highest annealing temperature used (240 °C) suggesting that n-butylamine is difficult to be removed completely from the spin-coated films as was similarly reported in the literature in the case of spin-coated films using propylamine [35, 41, 42]. Presence of n-butylamine in the annealed films could be alternatively observed from comparison with the data reported for the bulk $Ge_{25}S_{75}$ [43] where n (632.8 nm) = 2.132 and E_g = 2.47 eV. From our measurements even for annealing temperature 240 °C: n (632.8 nm) = 1.993 (see Fig. 4) and E_g = 3.13 eV (see Table 3) both still far from the bulk data.

Conclusions

Spectroscopic ellipsometry study was conducted on the non-toxic spin-coated amorphous $Ge_{25}S_{75}$ films annealed at different temperatures. The refractive index and extinction coefficient of those films over the

broad spectral range of the MIR-VIS-UV region ($0.05 < E < 6.0$ eV) were obtained by the best fit of ellipsometry data. Different model dielectric functions including Tauc-Lorentz oscillator or Cody-Lorentz oscillator for description of short wavelength absorption edge, and Lorentz or Gauss oscillators for description of phonon absorptions and optically active absorptions in MIR part of spectra were used and discussed.

Using a Mott-Davis model in the vicinity of the absorption edge ($3.0 < E < 4.0$ eV), the width of the localized states is decreasing indicating the decrease of local disorder with annealing temperature. Using Wemple-DiDomenico single oscillator dispersion in the semi-transparent spectrum ($0.5 < E < 2.5$ eV), the intensity of interband optical transition, E_d, shows an increase ~ 3 eV from as-prepared sample to the sample annealed at the highest temperature probably due to change of local arrangement around Ge cation connected with releasing of alkyl ammonium germanium salts residue from the film and thermo-induced polymerization. The energy of the effective dispersion oscillator (E_0) decreases with increasing annealing temperature indicating contraction of centroids of the valence and conduction bands. Some absorption in the MIR part of spectra especially that close to 3000 cm^{-1} could be associated to alkyl ammonium germanium salts in the spin-coated film. Decrease of its intensity correspond to results from EDS [8] and can be taken as alternative method to evaluation of spin-coated film quality.

In this article, the possibilities of spectroscopic ellipsometry in solid state chemistry especially for amorphous chalcogenides had been discussed. Comparison of different models for ellipsometry data evaluation reveal that although Cody-Lorentz model is closer to the expected results from electronic structure, Tauc-Lorentz model describe short wavelength edge with lower number of free parameters and moreover with lower mean square error. In the MIR part of spectra results obtained using Lorentz or Gauss oscillators are practically identical.

Acknowledgements: Authors appreciate financial support from project No. 16-13876S financed by the Grant Agency of the Czech Republic (GA CR) as well as support from the grants LM2015082 and CZ.1.05/4.1.00/11.0251 from the Ministry of Education, Youth and Sports of the Czech Republic.

References

[1] A. Stronski, M. Vlcek, A. Sklenar. *Quant. Electron. Optoelectron* **3**, 394 (2000).
[2] A. Zoubir, M. Richardson, C. Rivero, A. Schulte, C. Lopez, K. Richardson, N. Hô, R. Vallee. *Opt. Lett.* **29**, 748 (2004).
[3] S. Song, S. S. Howard, Z. Liu, A. O. Dirisu, C. F. Gmachl, C. B. Arnold. *Appl. Phys. Lett.* **89**, 041115 (2006).
[4] K. Tanaka, K. Shimakawa. *Amorphous Chalcogenide Semiconductors and Related Materials*. Springer, New York (2011).
[5] K. Palka, T. Syrovy, S. Schröter, S. Brückner, M. Rothhardt, M. Vlcek. *Opt. Mater. Express* **4**, 384 (2014).
[6] S. Novak, D. E. Johnston, Ch. Li, W. Deng, K. Richardson. *Thin Solid Films* **588**, 56 (2015).
[7] S. Slang, K. Palka, L. Loghina, A. Kovalskiy, H. Jain, M. Vlcek. *J. Non-Cryst. Solids* **426**, 125 (2015).
[8] S. Slang, P. Janicek, K. Palka, M. Vlcek. *Opt. Mater. Express* **6**, 1973 (2016).
[9] L. Tichy, H. Ticha, K. Handlir, K. Jurek. *J. Non-Cryst. Solids* **101**, 223 (1988).
[10] A. Vidourek, L. Tichy, M. Vlcek. *Mater. Lett.* **32**, 241 (1997).
[11] M. Munzar, L. Tichy, H. Ticha. *Curr. Appl. Phys.* **2**, 181 (2002).
[12] P. Knotek, L. Tichy, D. Arsova, Z. G. Ivanova, H. Ticha. *Mater. Chem. Phys.* **119**, 315 (2010).
[13] R. K. Pan, H. Z. Tao, H. C. Zang, C. G. Lin, T. J. Zhang, X. J. Zhao. *J. Non-Cryst. Solids* **357**, 2358 (2011).
[14] I. Ohlidal, D. Franta, M. Siler, F. Vizda, M. Frumar, J. Jedelsky, J. Omasta. *J. Non-Cryst. Solids* **352**, 5633 (2006).
[15] G. E. Jellison, Jr. F. A. Modine. *Appl. Phys. Lett.* **69**, 371 (1996).
[16] G. E. Jellison, Jr. F. A. Modine. *Appl. Phys. Lett.* **69**, 2137 (1996).
[17] A. S. Ferlauto, G. M. Ferreira, J. M. Pearce, C. R. Wronski, R. W. Wronski, X. Deng, G. Ganguly. *J. Appl. Phys.* **92**, 2424 (2002).
[18] G. C. Chern, I. Lauks. *J. Appl. Phys.* **53**, 6979 (1982).
[19] G. C. Chern, I. Lauks, A. R. McGhie. *J. Appl. Phys.* **54**, 4596 (1983).
[20] F. Wooten. *Optical Properties of Solids*. Academic Press, New York (1972).
[21] D. De Sousa Meneses, M. Malki, P. Echegut. *J. Non-Cryst. Solids* **351**, 769 (2006).
[22] K. -E. Peiponen, E. M. Vartiainen. *Phys. Rev. B* **44**, 8301 (1991).
[23] T. Kohoutek, J. Orava, J. Prikryl, T. Wagner, M. Frumar. *J. Non-Cryst. Solids* **357**, 157 (2011).
[24] C. M. Herzinger, B. Johs, W. A. McGahan, J. A. Woollam, W. Paulson. *J. Appl. Phys.* **83**, 3323 (1998).

[25] D. A. G. Bruggeman. *Ann. Phys. (Leipzig)* **24**, 636 (1935).
[26] Y. Zou, H. Lin, O. Ogbuu, L. Li, S. Danto, S. Novak, J. Novak, J. D. Musgraves, K. Richardson, J. Hu. *Opt. Mater. Express* **2**, 1723 (2012).
[27] M. Waldmann, J. D. Musgraves, K. Richardson, C. B. Arnold. *J. Mater. Chem.* **22**, 17848 (2012).
[28] L. Anghinolfi, M. Prato, A. Chtanov, M. Gross, A. Chincarini, M. Neri, G. Gemme, M. Canepa. *J. Phys. D: Appl. Phys.* **46**, 455301 (2013).
[29] R. de L. Kronig. *J. Opt. Soc. Am.* **12**, 547 (1926).
[30] H. A. Kramers. *Atti Cong. Intern. Fisici, (Transactions of Volta Centenary Congress) Como.* **2**, 545 (1927).
[31] S. H. Wemple. *Phys. Rev. B* **7**, 3767 (1973).
[32] S. H. Wemple, M. DiDomenico. *Phys. Rev. B* **3**, 1338 (1971).
[33] K. Tanaka. *Thin Solid Films* **66**, 271 (1980).
[34] H. Ticha, L. Tichy. *J. Optoelectron. Adv. Mater.* **4**, 381 (2002).
[35] S. Song, J. Dua, C. B. Arnold. *Opt. Express* **18**, 5472 (2010).
[36] N. F. Mott, E. A. Davis. *Electronic Processes in Non-Crystalline Materials*. Clarendon Press, Oxford (1979).
[37] E. A. Davis, N. F. Mott. *Phil. Mag.* **22**, 0903 (1970).
[38] J. Tauc. in *Amorphous and liquid semiconductors*, J. Tauc (Ed.), Plenum Press, New York (1974).
[39] S. R. Ovshinsky, D. Adler. *Contemp. Phys.* **19**, 109 (2006).
[40] M. L. Theye. in *Proceeding of the Fifth International Conference on Amorphous and Liquid Semiconductors*, Garmisch-Partenkirchen (1973).
[41] T. Kohoutek, J. Orava, L. Strizik, T. Wagner, A. L. Greer, M. Bardosova, H. Fudouzi. *Opt. Mater.* **36**, 390 (2013).
[42] Y. Zha, M. Waldmann, C. B. Arnold. *Opt. Mater. Express* **3**, 1259 (2013).
[43] J. P. Bérubé, S. H. Messaddeq, M. Bernier, I. Skripachev, Y. Messaddeq, R. Vallée. *Opt. Express* **22**, 26103 (2014).